Earthq Eng & Eng Vib (2016) 15: 657-672 **DOI**: 10.1007/s11803-016-0356-7

Analytical and numerical studies on the nonlinear dynamic response of orthotropic membranes under impact load

Liu Changjiang[1, 2 †], Zheng Zhoulian[3‡] and Yang Xiaoyan[4§]

1. *State Key Laboratory of Geohazard Prevention and Geoenvironment Protection, Chengdu University of Technology, Chengdu 610059, China*
2. *College of Environment and Civil Engineering, Chengdu University of Technology, Chengdu 610059, China*
3. *College of Civil Engineering, Chongqing University, Chongqing 400045, China*
4. *College of Nuclear Technology and Automation Engineering, Chengdu University of Technology, Chengdu 610059, China*

Abstract: Orthotropic membrane components and structures are widely used in building structures, instruments and meters, electronic engineering, space and aeronautics, etc., because of their light weights. However, the same lightweight combined with low stiffness make membranes prone to vibration under dynamic loads, and in some cases the vibration may lead to structural failure. Herein, the undamped nonlinear vibration response of pretension rectangular orthotropic membrane structures subjected to impact loading is studied by analytical and numerical methods. The analytical solution is obtained by solving the governing equations by the Bubnov-Galerkin method and the Lindstedt-Poincaré perturbation method. Numerical analysis has also been carried out based on the same theoretical model. The analytical and numerical results have been compared and analyzed, and the influence of various model parameters on membrane vibration discussed. The results obtained herein provide some theoretical basis for the vibration control and dynamic design of orthotropic membrane components and structures.

Keywords: membrane; nonlinear vibration; numerical analysis; impact load; parameter analysis

1 Introduction

Orthotropic membrane components and structures are widely used in building structures, instruments and meters, electronic engineering, etc. Membrane structures are very sensitive to impact loads (such as rainstorm, hails, drops) due to their lightweight and flexibleness; the loading sets off vibration in the membranes, which may lead to structural failure. Therefore, it is necessary to study the behavior of membrane structures under impact load so as to understand its basic response characteristics and to establish a computational basis for safety design.

Seventeenth century researchers laid the physical foundation and provided mathematical tools for dealing with membrane vibration. By the 18th century vibration mechanics has gained independence from physics, and the most important achievement is the evolution of linear vibration theory. In 1829, Poisson solved the linear free vibration problem for thin membranes (Chen and Liu, 1997). Nonlinear membrane vibration problems have also been studied. Qian (1982) studied the vibration of rectangular, circular and elliptical membranes with unequal tension in two directions and obtained an approximate solution for the free vibration frequencies. Yuan and Zhang (1993a, b) studied the large deflection and free vibration problem by the finite element method of lines. York *et al*. (1999) extended the material-point method (MPM) to handle membranes, which constituted a significant improvement over existing methods. Lin *et al*. (2008) obtained an analytical solution for free vibration of an annular membrane. Zheng *et al*. (2009) and Liu *et al*. (2010, 2013, 2014) considered the geometric nonlinearity of membranes and studied the vibration problem of orthotropic membranes with large deflection theory and analytical methods. Sunny *et al*. (2012) studied the nonlinear transverse vibration problem of a pre-stressed membrane by the Adomian decomposition method. Also, design issues concerning nonlinear vibration frequencies of rectangular orthotropic membranes were discussed by Wetherhold and Padliya (2014). Khan *et al*. (2014) studied the nonlinear behavior of the fabrication and characterization

Correspondence to: Liu Changjiang, State Key Laboratory of Geohazard Prevention and Geoenvironment Protection and College of Environment and Civil Engineering, Chengdu University of Technology, Chengdu 610059, China
Tel: +86-13880428142
E-mail: changjiangliucd@126.com
†Associate Professor; ‡Professor; §PhD

Supported by: National Natural Science Foundation of China under Grant No. 51178485 and the Personnel Development Project for Young and Middle-aged Key Teachers of Chengdu University of Technology under Grand No. KYGG201303
Received August 10, 2015; **Accepted** December 27, 2015

of a vibration-based polydimethylsiloxane membrane type electromagnetic energy harvester, and the results provided a useful basis for the actual engineering. Gajbhiye *et al*. (2015) studied the rectangular, flat thin membrane using PVDF piezo-actuated material as an actuator/sensor by the finite-element method.

Present studies on forced vibration caused by external loads have concentrated mainly on wind induced vibration. Many scholars carried out research on the theoretical analysis, numerical calculation and wind tunnel test of various forms of membrane structures (Shen and Wu, 2006; Matsumoto, 1990; Buchholdt, 1998; Yasui *et al*., 1999; Glück *et al*., 2003; Wu and Shen, 2003; Qin *et al*., 2008; Zhou *et al*., 2013; Chen *et al*., 2015). However, little research on the dynamic response of membrane structures under concentrated impact load has been done. Leigh and Porwal (2003) developed an analytical model for the ballistic impact response of fibrous materials of interest in body armor applications, and the comparison between the analytical and experimental results raised fundamental questions on many long-held views on the impact behavior of fabric systems. Suhir *et al*. (2009) studied the response of a 'flexible-and-heavy' square simply supported printed circuit board (PCB) to an impact drop load applied to its support contour and evaluated some major parameters of this response; significant results were obtained for engineering practice. Zheng *et al*. (2012) and Liu *et al*. (2014) studied the dynamic response of orthotropic membranes by analytical methods, but they didn't carry out numerical or experimental study to prove the correctness of their results. In addition, they didn't analyze the influence of each parameter on the vibration of the membrane.

In this paper we present a numerical study and parameter analysis of the dynamic response of membranes subjected to concentrated impact loads. Membrane structures usually remain elastic in actual application despite large deformations in the vibration process. Hence, we devoted our study to the elastic, but geometrically nonlinear, forced vibration of orthotropic membranes.

2 Governing equations and boundary conditions

Assume that the rectangular membrane is simply supported on its four edges and the membrane material is orthotropic. Its two orthogonal directions are the two principal fiber directions denoted by x and y in Fig.1, respectively, and a and b are the x and y dimensions. N_{0x} and N_{0y} are the initial tensions in the x and y directions, respectively. Assume that the impact loading comes from a pellet which can be considered a particle with mass M and initial velocity v_0, and the impact contact point is (x_0, y_0) as noted in the figure.

According to Von Kármán's large deflection theory and the D'Alembert principle (Zheng *et al*., 2009; Liu *et al*., 2010), the forced vibration partial differential equation and consistency equation for an orthotropic membrane are:

$$\begin{cases} \rho\dfrac{\partial^2 w}{\partial t^2}-(N_x+N_{0x})\dfrac{\partial^2 w}{\partial x^2}-(N_y+N_{0y})\dfrac{\partial^2 w}{\partial y^2}=p(x,y,t) \\ \dfrac{1}{E_1 h}\dfrac{\partial^2 N_x}{\partial y^2}-\dfrac{\mu_2}{E_2 h}\dfrac{\partial^2 N_y}{\partial y^2}-\dfrac{\mu_1}{E_1 h}\dfrac{\partial^2 N_x}{\partial x^2}+\dfrac{1}{E_2 h}\dfrac{\partial^2 N_y}{\partial x^2}-\dfrac{1}{Gh}\dfrac{\partial^2 N_{xy}}{\partial x\partial y}=\left(\dfrac{\partial^2 w}{\partial x\partial y}\right)^2-\dfrac{\partial^2 w}{\partial x^2}\dfrac{\partial^2 w}{\partial y^2} \end{cases} \tag{1}$$

where ρ denotes aerial density of membrane; N_x and N_y denote additional tension in x and y direction, respectively; N_{0x} and N_{0y} denote initial tension in x and y direction, respectively; N_{xy} denotes shear force; $w = w(x, y, t)$ denotes the deflection; $p(x, y, t)$ denotes the impact loading; h denotes membrane thickness. E_1 and E_2 denote Young's modulus in x and y direction, respectively. G denotes shearing modulus. μ_1 and μ_2 denote Poisson's ratio in x and y direction, respectively.

The pellet impact loading on the membrane can be expressed as follows:

$$p(x,y,t)=F(t)\delta(x-x_0)\delta(y-y_0) \tag{2}$$

where $F(t)$ denotes the impact force on the membrane; δ denotes the Dirac function.

According to the theorem of momentum, we obtain

$$F(t)=-M\frac{\partial w^2(x_0,y_0,t)}{\partial t^2} \tag{3}$$

The membrane is a plane before impact. Therefore, the initial condition of the membrane is

$$w(x_0,y_0,t)\big|_{t=0}=0,\quad \left.\frac{\partial w(x_0,y_0,t)}{\partial t}\right|_{t=0}=v_0' \tag{4}$$

where v_0' denotes the velocity of membrane at the time of $t = 0$.

The corresponding displacement and stress boundary conditions of the governing equations can be expressed as follows:

$$\begin{cases} w(0,y,t)=0,\ \dfrac{\partial^2 w}{\partial x^2}(0,y,t)=0 \\ w(a,y,t)=0,\ \dfrac{\partial^2 w}{\partial x^2}(a,y,t)=0 \end{cases} \quad \begin{cases} w(x,0,t)=0,\ \dfrac{\partial^2 w}{\partial y^2}(x,0,t)=0 \\ w(x,b,t)=0,\ \dfrac{\partial^2 w}{\partial y^2}(x,b,t)=0 \end{cases}$$

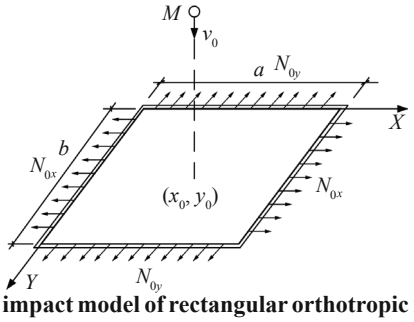

Fig. 1 The impact model of rectangular orthotropic membrane with four edges simply supported

(5)

$$\begin{cases} \dfrac{\partial^2\varphi}{\partial x^2}(0,y,t)=0 & \begin{cases} \dfrac{\partial^2\varphi}{\partial y^2}(x,0,t)=0 \\ \dfrac{\partial^2\varphi}{\partial y^2}(x,b,t)=0 \end{cases} \\ \dfrac{\partial^2\varphi}{\partial x^2}(a,y,t)=0 & \end{cases} \tag{6}$$

where φ denotes stress function $\varphi(x,y,t)$.

3 Analytical solution of the governing equations

The maximum vibration displacement of the membrane is much smaller than the boundary size, so the shearing actions among the membrane fibers are slight. Therefore, the effect of shearing stress is very small in the vibrating process of the membrane. In order to simplify the computation, we can take $N_{xy} = 0$. Meanwhile, introduce the stress function

$$\begin{cases} N_x = h\dfrac{\partial^2\varphi}{\partial y^2},\ N_{0x} = h\cdot\sigma_{0x} \\ N_y = h\dfrac{\partial^2\varphi}{\partial x^2},\ N_{0y} = h\cdot\sigma_{0y} \end{cases}$$

into Eq. (1), and Eq. (1) can be simplified as follows (Zheng *et al*., 2009; Liu *et al*., 2010):

$$\rho\frac{\partial^2 w}{\partial t^2} - h\left(\frac{\partial^2\varphi}{\partial y^2}+\sigma_{0x}\right)\frac{\partial^2 w}{\partial x^2} - h\left(\frac{\partial^2\varphi}{\partial x^2}+\sigma_{0y}\right)\frac{\partial^2 w}{\partial y^2} = p(x,y,t) \tag{7}$$

$$\frac{1}{E_1}\frac{\partial^4\varphi}{\partial y^4}+\frac{1}{E_2}\frac{\partial^4\varphi}{\partial x^4} = \left(\frac{\partial^2 w}{\partial x\partial y}\right)^2 - \frac{\partial^2 w}{\partial x^2}\frac{\partial^2 w}{\partial y^2} \tag{8}$$

where φ denotes stress function $\varphi(x,y,t)$, σ_{0x} and σ_{0y} denote initial tensile stress in x and y direction, respectively.

According to the vibration theory, assume that the functions that satisfy the boundary conditions (5) and (6) are

$$w(x,y,t) = \sum_{m=1}^{\infty}\sum_{n=1}^{\infty} T_{mn}(t)\cdot W_{mn}(x,y) \tag{9}$$

$$\varphi(x,y,t) = \sum_{m=1}^{\infty}\sum_{n=1}^{\infty} T_{mn}^2(t)\cdot \phi_{mn}(x,y) \tag{10}$$

where $W_{mn}(x, y)$ is the mode shape function, and $\phi_{mn}(x, y)$ and $T_{mn}(t)$ are unknown functions.

The mode shape function of rectangular membrane (Qian,1982) is

$$W_{mn}(x,y) = W(x,y) = \sin\frac{m\pi x}{a}\sin\frac{n\pi y}{b} \tag{11}$$

where m and n are integer, and denote the sine half-wave number in x and y, respectively. Equation (11) satisfies the displacement boundary condition (5) automatically. We can take one term of Eqs. (9) and (10) for computation, i.e.

$$w(x,y,t) = T(t)\cdot W(x,y) \tag{12}$$

$$\varphi(x,y,t) = T^2(t)\cdot\phi\ (x,y) \tag{13}$$

and then superpose the final results.

By substituting Eqs. (11), (12) and (13) into Eq. (8), one obtains

$$\frac{1}{E_1}\frac{\partial^4\phi}{\partial y^4}+\frac{1}{E_2}\frac{\partial^4\phi}{\partial x^4} = \frac{m^2n^2\pi^4}{2a^2b^2}\left(\cos\frac{2m\pi x}{a}+\cos\frac{2n\pi y}{b}\right) \tag{14}$$

Assume that the solution of Eq. (14) is given by

$$\phi(x,y) = \alpha\cdot\cos\frac{2m\pi x}{a}+\beta\cdot\cos\frac{2n\pi y}{b}+\gamma_1x^3+\gamma_2x^2+\gamma_3y^3+\gamma_4y^2 \tag{15}$$

The substitution of Eq. (15) into Eq. (14) yields

$$\alpha = \frac{E_2n^2a^2}{32m^2b^2},\ \ \beta = \frac{E_1m^2b^2}{32n^2a^2}$$

By substituting Eq. (15) into the stress boundary condition (6), one obtains

$$\gamma_1=\gamma_3=0,\ \ \gamma_2 = \frac{\pi^2E_2n^2}{16b^2},\ \ \gamma_4 = \frac{\pi^2E_1m^2}{16a^2}$$

By substituting α, β, γ_1, γ_2, γ_3 and γ_4 into Eq. (15), one obtains

$$\phi(x,y) = \frac{E_2n^2a^2}{32m^2b^2}\cos\frac{2m\pi x}{a}+\frac{E_1m^2b^2}{32n^2a^2}\cos\frac{2n\pi y}{b}+\frac{\pi^2E_2n^2}{16b^2}x^2+\frac{\pi^2E_1m^2}{16a^2}y^2 \tag{16}$$

The substitution of Eqs. (9), (10) and (16) into Eq. (7), and according to the Bubnov-Galerkin method, furnishes

$$\begin{aligned}&\iint_s\Big[\rho W^2\frac{\mathrm{d}^2T(t)}{dt^2}-h(\sigma_{0x}\frac{\partial^2W}{\partial x^2}W+\sigma_{0y}\frac{\partial^2W}{\partial y^2}W)T(t)-\\&h(\frac{\partial^2\phi}{\partial y^2}\frac{\partial^2W}{\partial x^2}W+\frac{\partial^2\phi}{\partial x^2}\frac{\partial^2W}{\partial y^2}W)T^3(t)\Big]\mathrm{d}x\mathrm{d}y\\&=\int_0^a\int_0^b\Big[F(t)\delta(x-x_0)(y-y_0)W(x,y)\Big]\mathrm{d}x\mathrm{d}y\end{aligned} \tag{17}$$

The substitution of Eq. (16) into Eq. (17) yields

$$\begin{aligned}&\int_0^a\int_0^b\Big[\rho W^2\frac{\mathrm{d}^2T(t)}{\mathrm{d}t^2}-(N_{0x}\frac{\partial^2W}{\partial x^2}W+N_{0y}\frac{\partial^2W}{\partial y^2}W)T(t)+\\&(h\frac{E_1m^2\pi^2}{4a^2}\sin^2\frac{n\pi y}{b}\cdot\frac{\partial^2W}{\partial x^2}W+h\frac{E_2n^2\pi^2}{4b^2}\sin^2\frac{m\pi y}{b}\frac{\partial^2W}{\partial y^2}W)T^3(t)\Big]\mathrm{d}x\mathrm{d}y\\&=\int_0^a\int_0^b\Big[F(t)\delta(x-x_0)(y-y_0)W(x,y)\Big]\mathrm{d}x\mathrm{d}y\end{aligned} \tag{18}$$

where

$$W=\sin\frac{m\pi x}{a}\sin\frac{n\pi y}{b},\ \frac{\partial^2 W}{\partial x^2}=-\frac{m^2\pi^2}{a^2}\sin\frac{m\pi x}{a}\sin\frac{n\pi y}{b},$$

$$\frac{\partial^2 W}{\partial y^2}=-\frac{n^2\pi^2}{b^2}\sin\frac{m\pi x}{a}\sin\frac{n\pi y}{b},$$

$$W^2=\sin^2\frac{m\pi x}{a}\sin^2\frac{n\pi y}{b}=\frac{1}{4}(1-\cos\frac{2m\pi x}{a})(1-\cos\frac{2n\pi y}{b})$$

The substitution of all the aforementioned expressions into Eq. (18) results in

$$\rho\frac{ab}{4}\cdot\frac{\mathrm{d}^2T(t)}{\mathrm{d}t^2}+(\frac{m^2\pi^2b}{4a}\cdot N_{0x}+\frac{n^2\pi^2a}{4b}\cdot N_{0y})T(t)+\frac{3m^2n^2\pi^4h\beta+3m^2n^2\pi^4h\alpha}{2ab}T^3(t)=F(t)W(x_0,y_0) \tag{19}$$

The substitution of the expression of $F(t)$, namely Eq. (3), into Eq. (19) and after simplifications yields

$$\frac{\mathrm{d}^2T(t)}{\mathrm{d}t^2}+\frac{m^2\pi^2b^2N_{0x}+n^2\pi^2a^2N_{0y}}{\rho a^2b^2+4abM\sin^2\frac{m\pi x_0}{a}\cdot\sin^2\frac{n\pi y_0}{b}}T(t)+\frac{6m^2n^2\pi^4h\beta+6m^2n^2\pi^4h\alpha}{\rho a^2b^2+4abM\sin^2\frac{m\pi x_0}{a}\cdot\sin^2\frac{n\pi y_0}{b}}T^3(t)=0 \tag{20}$$

It is clear that Eq. (20) is a nonlinear differential equation with respect to $T(t)$. It is very difficult to obtain an analytical solution of this equation. Therefore, we apply the L-P perturbation method to obtain an approximate analytic solution.

Because $(h^2/ab)<<1$ and it is a dimensionless parameter, we can take $\varepsilon=(h^2/ab)<<1$ as the perturbation parameter. Then Eq. (20) can be simplified as

$$\frac{\mathrm{d}^2T(t)}{\mathrm{d}t^2}+\omega_0^2\left[T(t)+\varepsilon\alpha_3T^3(t)\right]=0 \tag{21}$$

where $\omega_0^2=\dfrac{m^2\pi^2b^2N_{0x}+n^2\pi^2a^2N_{0y}}{\rho a^2b^2+4abM\sin^2\frac{m\pi x_0}{a}\cdot\sin^2\frac{n\pi y_0}{b}}$,

$$\alpha_3=\frac{6m^2n^2\pi^2(\alpha+\beta)}{h\left(m^2\frac{b}{a}N_{0x}+n^2\frac{a}{b}N_{0y}\right)}\ .$$

By introducing a new variable $\tau=\omega t$, we obtain

$$\frac{\mathrm{d}^2T(t)}{\mathrm{d}t^2}=\omega^2\frac{\mathrm{d}^2T(t)}{\mathrm{d}\tau^2} \tag{22}$$

Spread ω and $T(t)$ as a power series with respect to ε:

$$\omega=\omega_0+\varepsilon\omega_1+\varepsilon^2\omega_2+0(\varepsilon^3) \tag{23}$$

$$T(t)=T_0(\tau)+\varepsilon T_1(\tau)+\varepsilon^2T_2(\tau)+0(\varepsilon^3) \tag{24}$$

The substitution of Eq. (22), (23), (24) into Eq. (21) yields

$$(\omega_0+\varepsilon\omega_1+\varepsilon^2\omega_2+\cdots)^2(\frac{\mathrm{d}^2T_0(\tau)}{\mathrm{d}\tau^2}+\varepsilon\frac{\mathrm{d}^2T_1(\tau)}{\mathrm{d}\tau^2}+\varepsilon^2\frac{\mathrm{d}^2T_1(\tau)}{\mathrm{d}\tau^2}+\cdots)+\omega_0^2(T_0(\tau)+\varepsilon T_1(\tau)+\varepsilon^2T_2(\tau)+\cdots)=-\omega_0^2\varepsilon\alpha_3(T_0(\tau)+\varepsilon T_1(\tau)+\varepsilon^2T_2(\tau)+\cdots)^3 \tag{25}$$

Take the first power of ε as an approximation. Spread Eq. (25), and compare the coefficient of each power of ε yields

$$\omega_0^2\frac{\mathrm{d}^2T_0(\tau)}{\mathrm{d}\tau^2}+\omega_0^2T_0(\tau)=0 \tag{26}$$

$$\varepsilon^1:\omega_0^2\frac{\mathrm{d}^2T_1(\tau)}{\mathrm{d}\tau^2}+2\omega_0\omega_1\frac{\mathrm{d}^2T_0(\tau)}{\mathrm{d}\tau^2}+\omega_0^2T_1(\tau)=-\omega_0^2\alpha_3T_0(\tau)^3 \tag{27}$$

where $T_0(\tau)$, $T_1(\tau)$ satisfy the periodic condition $T_i(\tau+2\pi)=T_i(\tau)$, $i=1,2\cdots$.

The membrane has zero initial displacement when $t=0$, so let the initial condition is

$$T_i(0)=0,\ \ i=1,2\cdots \tag{28}$$

By solving Eq. (26) with the initial condition of (28), one obtains

$$T_0(\tau)=A\cdot\sin\tau \tag{29}$$

where A is a constant.

The substitution of Eq. (29) into Eq. (27) yields

$$\omega_0^2\frac{\mathrm{d}^2T_1(\tau)}{\mathrm{d}\tau^2}-2A\omega_0\omega_1\sin\tau+\omega_0^2T_1(\tau)=-\omega_0^2\alpha_3A^3\sin^3\tau \tag{30}$$

According to the trigonometric formula:

$\sin^3\tau=\frac{3}{4}\sin\tau-\frac{1}{4}\sin3\tau$, Eq. (30) can be transformed into

$$\frac{\mathrm{d}^2T_1(\tau)}{\mathrm{d}\tau^2}+T_1(\tau)=\frac{A}{4\omega_0}(8\omega_1-3A^2\alpha_3\omega_0)\sin\tau+\frac{1}{4}A^3\alpha_3\sin3\tau \tag{31}$$

Equation (31) is a linear forced vibration equation, with a homogeneous solution

$$g=B_1\cos\tau+B_2\sin\tau$$

where B_1 and B_2 are two constants.

The inhomogeneous term of Eq. (31) is

$$f=\frac{A}{4\omega_0}(8\omega_1-3A^2\alpha_3\omega_0)\sin\tau+\frac{1}{4}A^3\alpha_3\sin3\tau$$

According to the perturbation theory, in order to make the general solution of Eq. (31) not contain secular terms, we must orthogonalize *g* and *f*, i.e.

$$\langle g, f \rangle = \frac{1}{2\pi}\int_0^{2\pi} g \cdot f \,\mathrm{d}\tau = 0 \tag{32}$$

The substitution of *g* and *f* into Eq. (32) yields

$$\omega_1 = \frac{3\omega_0\alpha_3 A^2}{8}$$

By applying the initial condition of (28) to Eq. (27), one obtains

$$T_1(\tau) = B\sin\tau - \frac{\alpha_3 A^3}{32}\sin 3\tau \tag{33}$$

where *B* is also a constant.

The substitution of Eq. (29) and Eq. (33) into Eq. (24) yields

$$T(\tau) = T_0(\tau) + \varepsilon T_1(\tau) + 0(\varepsilon^2) = (A + \varepsilon B)\sin\tau - \frac{\varepsilon\alpha_3 A^3}{32}\sin 3\tau \tag{34}$$

By substituting $\tau = \omega t = (\omega_0 + \varepsilon\omega_1)t = \omega_0(1 + \frac{3\varepsilon\alpha_3 A^2}{8})t$ into Eq. (34), one obtains

$$T(t) = (A + \varepsilon B)\sin\omega t - \frac{\varepsilon\alpha_3 A^3}{32}\sin 3\omega t \tag{35}$$

where $\omega = \omega_0(1 + \frac{3\varepsilon\alpha_3 A^2}{8})$.

Now, we determine the constants *A* and *B* according to the initial conditions. The impact actuation duration of the pellet impacting the membrane is very short. So the system formed by the pellet and membrane can be considered as a conservative system. According to the principle of conservation of momentum, we can obtain the following expression

$$Mv_0 = Mv_0' + \iint_s \rho v_0' W(x, y)\mathrm{d}s \tag{36}$$

The substitution of Eq. (11) into Eq. (36) yields

$$v_0' = \frac{Mv_0}{M + \dfrac{4\rho ab}{\pi^2}} \tag{37}$$

The pellet and membrane have the same initial velocity v_0' at the time of $t = 0$. We can therefore obtain the following initial condition

$$\left.\frac{\partial w(x_0, y_0, t)}{\partial t}\right|_{t=0} = \sin\frac{m\pi x_0}{a}\cdot\sin\frac{n\pi y_0}{b}\cdot\left.\frac{\mathrm{d}T(t)}{\mathrm{d}t}\right|_{t=0} = v_0'$$

i.e.

$$\left.\frac{\mathrm{d}T(t)}{\mathrm{d}t}\right|_{t=0} = \frac{v_0'}{\sin\dfrac{m\pi x_0}{a}\cdot\sin\dfrac{n\pi y_0}{b}} \tag{38}$$

The substitution of Eq. (35) into Eq. (38) yields

$$(A + \varepsilon B)\omega - \frac{3\varepsilon\alpha_3 A^3}{32}\omega = \frac{v_0'}{\sin\dfrac{m\pi x_0}{a}\cdot\sin\dfrac{n\pi y_0}{b}} \tag{39}$$

The substitution of Eq. (29) into Eq. (38) yields

$$A = \frac{v_0'}{\omega\sin\dfrac{m\pi x_0}{a}\cdot\sin\dfrac{n\pi y_0}{b}} \tag{40}$$

The substitution of Eq. (40) into Eq. (39) yields

$$B = \frac{3\alpha_3 v_0'^3}{32\omega^3\sin^3\dfrac{m\pi x_0}{a}\cdot\sin^3\dfrac{n\pi y_0}{b}} \tag{41}$$

By substituting Eq. (40) into $\omega_0(1 + \frac{3\varepsilon\alpha_3 A^2}{8}) = \omega$, and solving it, one obtains

$$\omega = \frac{\omega_0}{3} + \frac{2\cdot 2^{1/3}\cdot C^2\cdot\omega_0^2}{3\left(16C^6\omega_0^3 + 81C^4 v_0'^2\omega_0\alpha_3\varepsilon + 9\sqrt{32C^{10}v_0'^2\omega_0^4\alpha_3\varepsilon + 81C^8 v_0'^4\omega_0^2\alpha_3^2\varepsilon^2}\right)^{1/3}} + \frac{\left(16C^6\omega_0^3 + 81C^4 v_0'^2\omega_0\alpha_3\varepsilon + 9\sqrt{32C^{10}v_0'^2\omega_0^4\alpha_3\varepsilon + 81C^8 v_0'^4\omega_0^2\alpha_3^2\varepsilon^2}\right)^{1/3}}{6\cdot 2^{1/3}\cdot C^2} \tag{42}$$

where $C = \sin\dfrac{m\pi x_0}{a}\cdot\sin\dfrac{n\pi y_0}{b}$. Equation (42) is the formula for the vibration frequency.

The substitution of Eqs. (40) and (41) into Eq. (35) yields

$$T(t) = \left(\frac{v_0'}{\omega\sin\dfrac{m\pi x_0}{a}\cdot\sin\dfrac{n\pi y_0}{b}} + \frac{3\varepsilon\alpha_3 v_0'^3}{32\omega^3\sin^3\dfrac{m\pi x_0}{a}\cdot\sin^3\dfrac{n\pi y_0}{b}}\right)\sin\omega t - \frac{\varepsilon\alpha_3 v_0'^3}{32\omega^3\sin^3\dfrac{m\pi x_0}{a}\cdot\sin^3\dfrac{n\pi y_0}{b}}\sin 3\omega t \tag{43}$$

The substitution of Eq. (43) into Eq. (9) yields

$$w(x, y, t) = \sum_{m=1}^{\infty}\sum_{n=1}^{\infty} W_{mn}\left[\left(\frac{v_0'}{\omega\sin\dfrac{m\pi x_0}{a}\cdot\sin\dfrac{n\pi y_0}{b}} + \frac{3\varepsilon\alpha_3 v_0'^3}{32\omega^3\sin^3\dfrac{m\pi x_0}{a}\cdot\sin^3\dfrac{n\pi y_0}{b}}\right)\cdot\sin\omega t - \frac{\varepsilon\alpha_3 v_0'^3}{32\omega^3\sin^3\dfrac{m\pi x_0}{a}\cdot\sin^3\dfrac{n\pi y_0}{b}}\sin 3\omega t\right] \tag{44}$$

The substitution of Eq. (43) into Eq. (3) yields

$$F(t) = \sum_{m=1}^{\infty}\sum_{n=1}^{\infty} W_{mn} M\left[\left(\frac{v_0'\omega}{\sin\dfrac{m\pi x_0}{a}\cdot\sin\dfrac{n\pi y_0}{b}} + \frac{3\varepsilon\alpha_3 v_0'^3}{32\omega\sin^3\dfrac{m\pi x_0}{a}\cdot\sin^3\dfrac{n\pi y_0}{b}}\right)\sin\omega t - \frac{9\varepsilon\alpha_3 v_0'^3}{32\omega\sin^3\dfrac{m\pi x_0}{a}\cdot\sin^3\dfrac{n\pi y_0}{b}}\sin 3\omega t\right] \tag{45}$$

By finding the one and two time derivative of Eq. (44), one obtains

$$v(x,y,t)=\sum_{m=1}^{\infty}\sum_{n=1}^{\infty}W_{mn}[(\frac{v_0'}{\sin\frac{m\pi x_0}{a}\cdot\sin\frac{n\pi y_0}{b}}+\frac{3\varepsilon\alpha_3 v_0'^3}{32\omega^2\sin^3\frac{m\pi x_0}{a}\cdot\sin^3\frac{n\pi y_0}{b}})\cdot \cos\omega t-\frac{3\varepsilon\alpha_3 v_0'^3}{32\omega^2\sin^3\frac{m\pi x_0}{a}\cdot\sin^3\frac{n\pi y_0}{b}}\cos 3\omega t] \quad (46)$$

$$a(x,y,t)=\sum_{m=1}^{\infty}\sum_{n=1}^{\infty}W_{mn}[-(\frac{v_0'\omega}{\sin\frac{m\pi x_0}{a}\cdot\sin\frac{n\pi y_0}{b}}+\frac{3\varepsilon\alpha_3 v_0'^3}{32\omega\sin^3\frac{m\pi x_0}{a}\cdot\sin^3\frac{n\pi y_0}{b}})\cdot \sin\omega t+\frac{9\varepsilon\alpha_3 v_0'^3}{32\omega\sin^3\frac{m\pi x_0}{a}\cdot\sin^3\frac{n\pi y_0}{b}}\sin 3\omega t] \quad (47)$$

where $v(x,y,t)$ and $a(x,y,t)$ are the velocity and acceleration of the membrane, respectively.

4 Illustrative example of analytic solution

Consider a commonly used membrane material where the Young's modulus in x and y are E_1 = 1.4×10^6 kN/m^2 and E_2 = 0.9×10^6 kN/m^2, respectively. The aerial density of membranes is ρ = 1.7 kg/m^2. The example membrane has thickness h = 1.0 mm, length a = 0.4 m and width b = 0.2 m. The mass of the pellet is $M=10^{-2}$ kg. Pretensions are $N_{0x}=N_{0y}=10$kN/m .

4.1 Computation of frequencies

Frequencies of the first three orders under different pellet initial velocities are computed according to Eq. (42) and the results presented in Table 1.

We can make several observations based on the results in Table 1.

(1) The membrane frequency increases with increasing initial velocity of the pellet, and increasing vibration order.

(2) For each vibration mode, the frequency value is minimum when $v_0\to0$, i.e., it approaches the small amplitude (i.e. linear) free vibration frequency.

4.2 Displacement time histories of impact point

Take the center point of membrane (i.e. $x_0=a/2, y_0=b/2$) as the impact point. The displacement time histories of the impact point are analyzed according to Eq. (44). For v_0 = 15 m/s (25 m/s), the vibration time-history curves of the first three orders are shown in Fig. 2, where by the blue (red) dotted line.

Table 1 Values of frequency (rad/s) under different initial velocities of pellet

Order	Initial velocities of the pellet v_0 (m/s)					
	125	100	75	50	25	$v_0\to0$
First	1435.95	1400.47	1370.40	1347.26	1332.60	1327.57
Second	2344.56	2278.80	2222.35	2178.43	2150.33	2140.63
Third	3992.31	3870.70	3765.52	3682.98	3629.80	3611.37

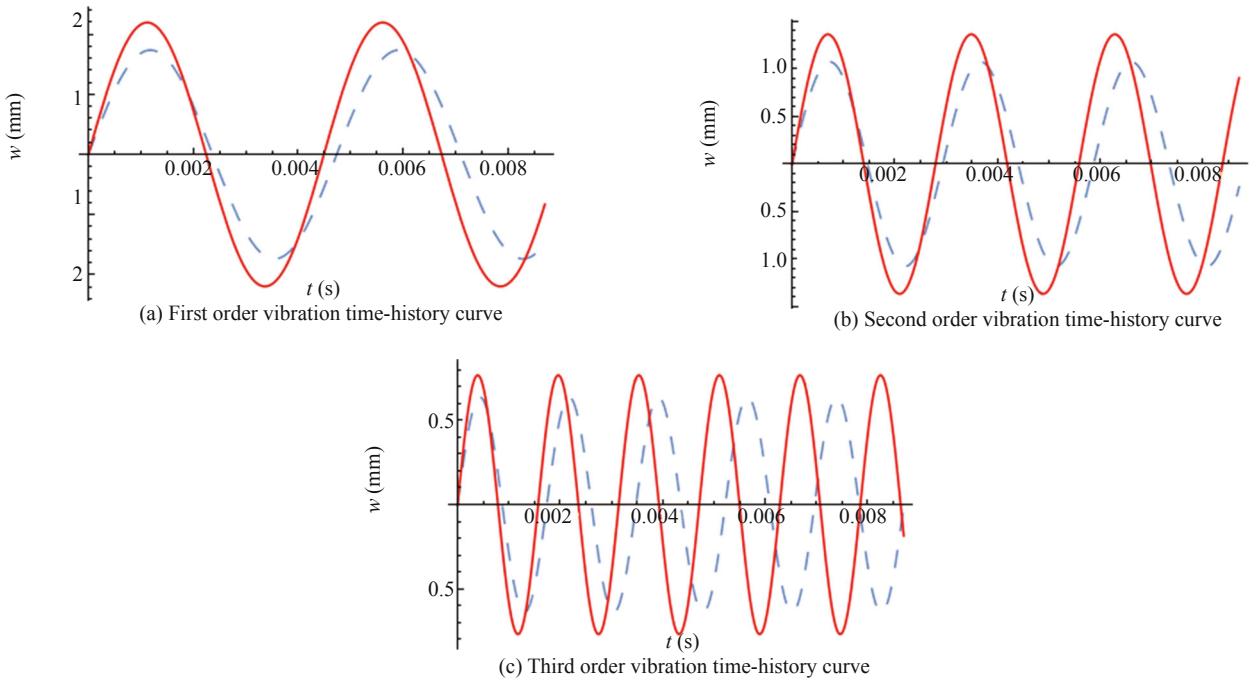

(a) First order vibration time-history curve

(b) Second order vibration time-history curve

(c) Third order vibration time-history curve

Fig. 2 The single mode displacement and time curves of the impact point of the membrane

From Fig. 2, we can make the following observations:

(1) The vibration period decreases with the increase of vibration order. The maximum amplitude decreases with the increase of vibration order.

(2) The maximum amplitude of each order increases with the increase of initial velocity of the pellet. This reflects the nonlinearity of the forced vibration of the membrane.

Figure 3 shows the vibration time-history curves of the impact point ($x_0 = a/2$, $y_0 = b/2$) according to Eq. (44) for pellet velocities of: $v_0 = 15$ m/s, $v_0 = 20$ m/s, $v_0 = 25$ m/s. The maximum displacement values of the impact point are shown in Table 2. One can conclude that the maximum displacement of the impact point increases with respect to increasing initial velocity of the pellet. The impact point did reciprocating motion after the pellet acts on the membrane, and the motion will continue (i.e., the vibration will not attenuate).

4.3 Analysis of vibration modes

We substituted the material and geometric parameters into Eq. (44) to obtain the displacement function of the vibration of each order. Assume that the initial velocity of the pellet is $v_0 = 15$ m/s and the time $t = 0.001$ s. The vibration modes of the first six orders according to these displacement functions are shown in Figs. 4-9. By superimposing the vibration modes of the first three orders, we can obtain the superposed vibration modes that are given in Fig. 10. The dimension of the coordinates of Figs. 4-9 is in meter.

From the results of the vibration mode analysis, we can conclude that one can expediently compute the vibration mode of each order by using the deflection

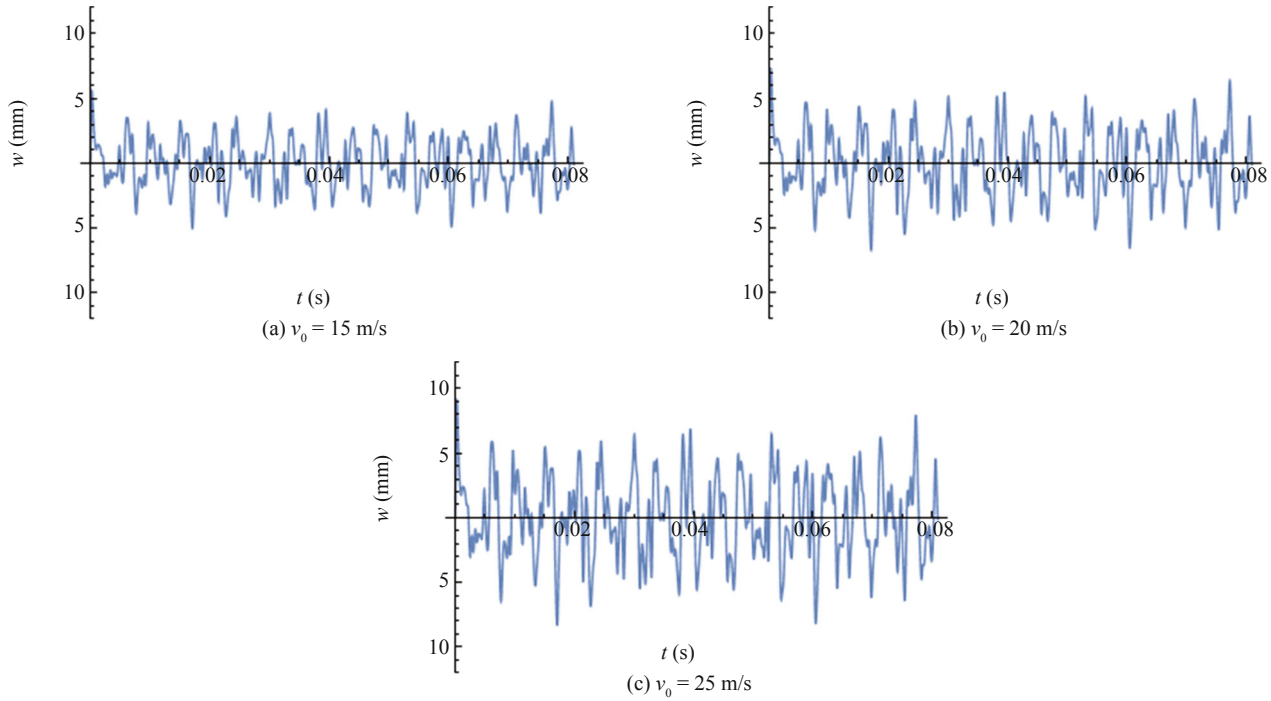

Fig. 3 Displacement and time curves of the impact point of the membrane

Table 2 Maximum displacement values of impact point

Initial velocity (m/s)	15	20	25
Maximum displacement (mm)	5.6	7.4	9.1

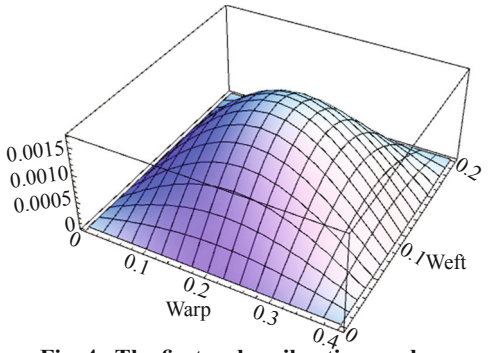

Fig. 4 The first order vibration mode

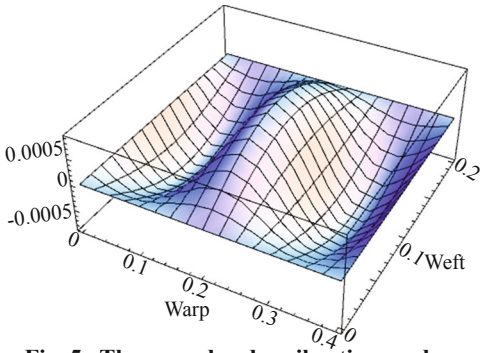

Fig. 5 The second order vibration mode

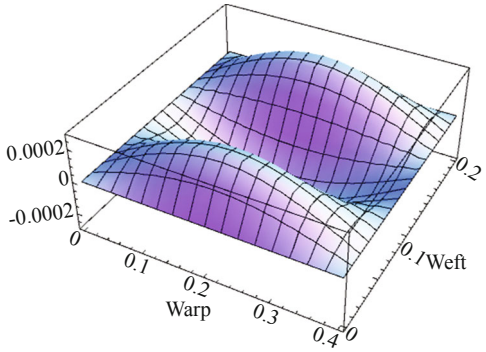

Fig. 6 The third order vibration mode

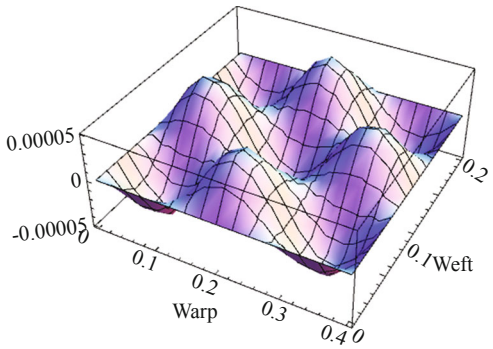

Fig. 7 The fourth order vibration mode

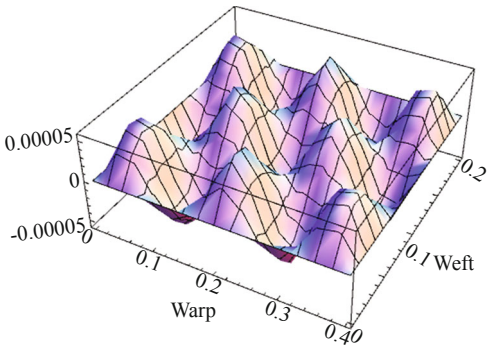

Fig. 8 The fifth order vibration mode

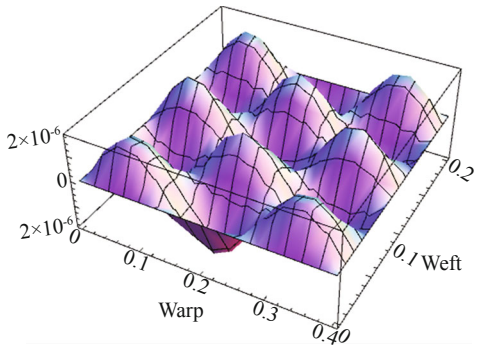

Fig. 9 The sixth order vibration mode

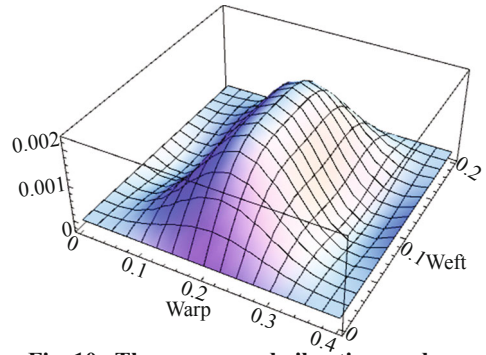

Fig. 10 The superposed vibration mode

function (44). In addition, the total superposed vibration mode of the nonlinear forced vibration of orthotropic membranes under concentrated impact load can be computed conveniently. The vibration amplitude decreases with respect to increasing vibration order, i.e. the contribution of the low order vibration modes is larger than the higher order vibration modes. Therefore, we just need to consider vibration modes of the first three to six orders. The total superposed vibration mode is axial-symmetric in the x and y directions.

5 Comparison and analysis of numerical and analytical results

5.1 Model of numerical analysis

The finite element analysis software ANSYS/LS-DYNA was used to analyze the nonlinear vibration of the pretension rectangular orthotropic membrane structure with four edges fixed under impact force. The impact force is imposed by a rigid pellet with an initial velocity. The solution method is implicit-explicit continuous solution. In the implicit solution, the membrane elements are represented by SHELL181 (only membrane algorithm) and pellet element is SOLID185 (3D solid). In the explicit solution, the elements convert into SHELL163 and SOLID164. In order to avoid hourglass in the computing process, the complete integral Belytschko-Tsay membrane algorithm was used for SHELL163.

The unit system of the numerical analysis is shown in Table 3. The material property parameters are the same as those of the analytic solution. The material property

Table 3 Unit prescribes of the numerical analysis

Mass	Length	Time	Force	Stress	Energy	Density	Young′s	Velocity
ton	mm	s	N	MPa	N·mm	t/mm^3	MPa	mm/s

Table 4 Material property parameters of the numerical model

Element	h/R(mm)	ρ (t/mm^3)	Ex (MPa)	Ey (MPa)	NUXY	Gt
Shell 181	1	1.7e-9	1400	900	0.3	12
Solid 185	10	1.91e-8	——	——	——	——

parameters are shown in Table 4.

5.2 Meshing and pretension

The four-node surface element is used in the mesh. The center area of the membrane surface is the main impacting area of the pellet, so the meshing of the center area is much finer. In order to meshing the pellet by using hexahedron mapping solid element, the pellet is split into eight one-eighth pellet by moving and revolving working plane. After meshing, the finite element model is shown in Fig. 11.

In the implicit analysis, the pretension of membrane is applied by applying the same displacement on the two opposite sides of rectangular membrane.

Because the elastic moduli in the two orthotropic directions are different, the principal axis direction of the element coordinate system must align with the direction of the global coordinate system. Aligning the fiber directions with the x and y directions of the coordinate system, the stress-strain relationship of the membrane is

$$\left.\begin{aligned}\varepsilon_x &= \frac{1}{E_1 h}N_x - \frac{\mu_2}{E_2 h}N_y \\ \varepsilon_y &= \frac{\mu_1}{E_1 h}N_x - \frac{1}{E_2 h}N_y\end{aligned}\right\} \tag{48}$$

The displacement in x and y direction is

$$\left.\begin{aligned}\Delta l_x &= \varepsilon_x l_x \\ \Delta l_y &= \varepsilon_y l_y\end{aligned}\right\} \tag{49}$$

where ε_x and ε_y denote the strains of x and y directions, respectively; h denotes the thickness of membrane; E_1 and E_2 denote the elastic modulus in x and y direction, respectively; μ_1 and μ_2 denote Poisson's ratio in x and y direction, respectively; N_x and N_y denote the pretension of x and y direction, respectively; l_x and l_y denote the length of x and y direction, respectively; Δl_x and Δl_y denote the displacement of x and y direction, respectively.

The corresponding displacement of N_x and N_y can be obtained by Eqs. (48) and (49). Then the pretension of membrane can be exerted by imposing the corresponding displacement in the x and y direction, respectively.

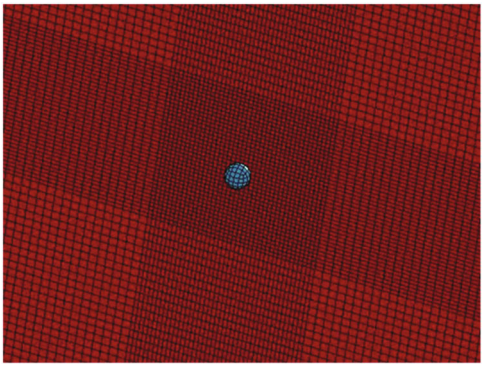

Fig. 11 Membrane surface grid division and spheroid grid division

5.3 The solving process

Firstly, implicit solving was carried out. The complete restrictions were applied to all nodes of the pellet element. The corresponding displacements calculated by Eq. (49) were imposed on the membrane. Then, the keyword file of implicit solving was submitted to LS-DYNA to carry out the explicit solving. In explicit solving, the membrane elements change to SHELL163 and the pellet elements change to SOLID164.

In order to avoid penetration between the pellet and membrane elements, density of the elements in the contact area and the stiffness of penalty function were increased, and the contact thickness was decreased. Through this adjustment the penalty factor was determined as 0.8.

The solution of the model leads to the post-processing stage. The post-processing software is LS-PREPOST.

In the numerical analysis the parameters of the membrane and pellet are the same as those in Section 3. The displacement time history and maximum displacement of the impact point $(a/2, b/2)$ are calculated in the numerical analysis. Meanwhile, the results of the numerical and theoretical calculations are compared and analyzed.

5.4 Comparative analysis of frequencies

The analytical and numerical frequencies of the first three orders for various pellet initial velocities are compared in Table 5. It is observed that:

(1) All frequencies, analytical and numerical, increase with the increase of pellet initial velocity and the vibration orders.

(2) The relative difference between the analytical and numerical results also increases with the increase of pellet initial velocity and the vibration orders. But the relative differences are all less than 5% within the first three orders.

5.5 Comparative analysis of displacement time histories

Displacement time histories of the impact point obtained from the analytical calculation and numerical analysis are shown in Fig. 12 (time in second, and displacement in mm). It can be seen that the displacement time histories from analytical calculation is very close to those from numerical analysis. Only the theoretical value of the maximum displacement of the impact point is slightly less than the numerical value. This proves the correctness of the analytical solution.

5.6 Comparative analysis of maxium displacements

The analytical and numerical results of the maximum displacement of the membrane are compared and analyzed; the deformation diagrams are shown in Fig. 13 and 14 while the displacement values are listed in

Table 5 Values of frequency (rad/s) under different initial velocities of pellet

Order		Initial velocities of the pellet v_0 (m/s)			
		75	50	25	$v_0 \to 0$
First	Analytical	1370.40	1347.26	1332.60	1327.57
	Numerical	1310.80	1295.30	1290.12	1288.35
	Relative difference (%)	4.55	4.01	3.30	3.04
Second	Analytical	2222.35	2178.43	2150.33	2140.63
	Numerical	2123.40	2092.43	2079.62	2074.27
	Relative difference (%)	4.66	4.11	3.40	3.20
Third	Analytical	3765.52	3682.98	3629.80	3611.37
	Numerical	3594.77	3534.53	3507.73	3495.67
	Relative difference (%)	4.75	4.20	3.48	3.31

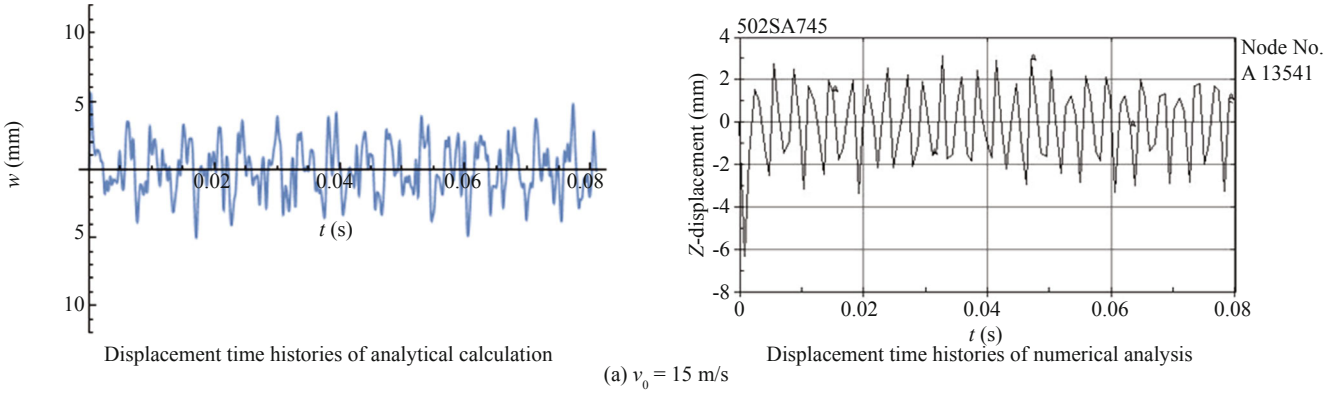

(a) v_0 = 15 m/s

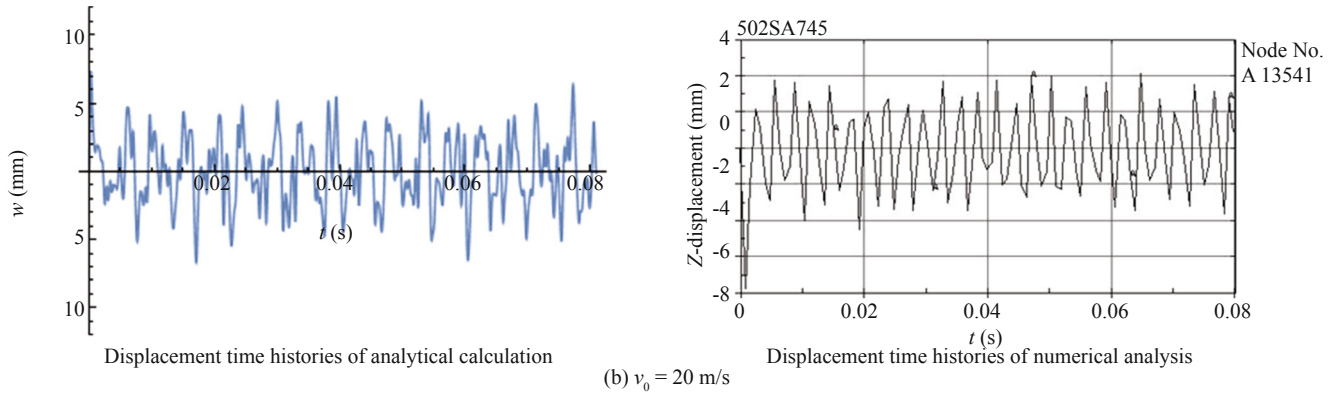

(b) v_0 = 20 m/s

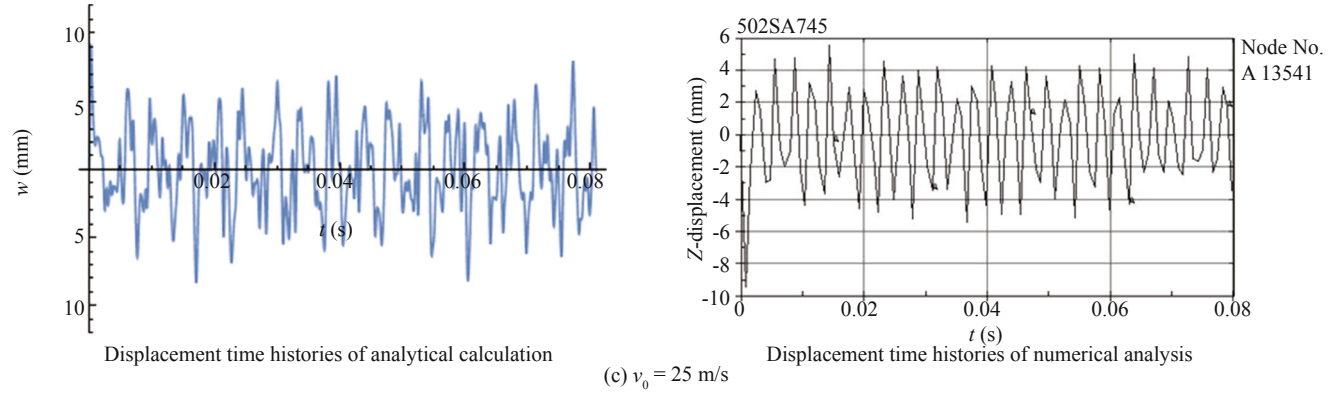

(c) v_0 = 25 m/s

Fig. 12 Displacement time histories of the impact point of the membrane

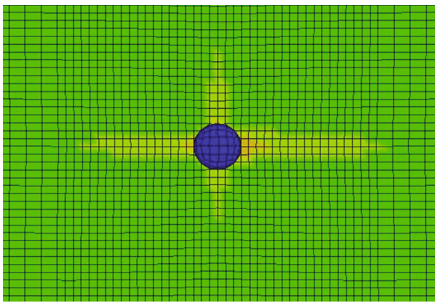

Fig. 13 The plan view of the deformation of the membrane

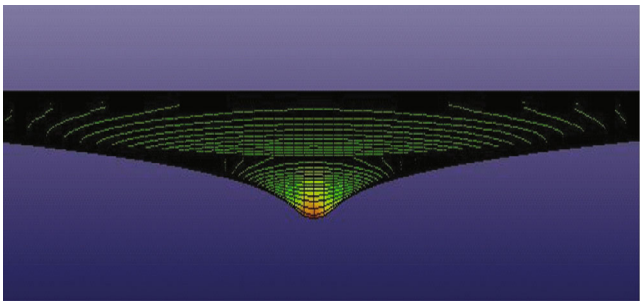

Fig. 14 The lateral view of the deformation of the membrane

Table 6 Comparison of analytical and numerical results of the maximum displacement

Velocity	v_0 = 15 m/s	v_0 = 15 m/s	v_0 = 15 m/s
Analytical results (mm)	5.60	7.40	9.10
Numerical results (mm)	6.1296	7.7247	9.1287
Relative difference (%)	9.46	4.39	0.32

Table 6, together with their relative differences.

From Table 6 it can be seen that the relative differences in the maximum displacement results are small, with a maximum value of 9.46%. Hence, the numerical results are in good agreement with the analytical results. It can be seen also from Table 6 that the relative difference between the analytical and numerical results decreases with the increase of the initial velocity of the pellet, and the analytical results are slightly less than the numerical results. The reason is as follows:

(1) In order to eliminate stress singularity of the membrane under the concentrated load, the smooth sine function is taken as the displacement function there without fully considering the deformation characteristics of the membrane under the pellet.

(2) In reality there is a displacement amplification effect in the area near the impact point on the membrane. A side view of the membrane deformation under the pellet is shown in Fig. 15 which shows clearly the amplification in the area near the impact point. The shape function of the analytical solution cannot precisely express this amplified deformation so the results of the analytical calculation are slightly smaller than the of numerical analysis results.

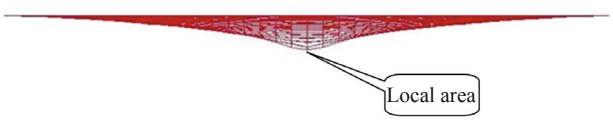

Fig. 15 The side view of the membrane deformation under the pellet impact

(3) With increasing initial pellet velocity, this local amplification effect is gradually weakened since the relative difference between the analytical and numerical displacements decreases as the initial pellet velocity increases.

6 Analysis of the influence of parameters

Boundary size, pretension and surface density of the membrane, and the velocity and quality of the pellet all have an influence on membrane vibration. The effects of these parameters are analyzed by comparing the numerical and analytical results on the maximum displacement.

6.1 Membrane size

To analyze the influence of membrane size, analytical and numerical results on the maximum displacement of the impact point for selected membrane dimensions are collected in Table 7 and Fig. 16. The calculation parameters are taken as: h = 1 mm, ρ = 1.7 kg/m^2, $M = 10^{-3}$ kg, $E_1 = 1.4\times10^6$ kN/m^2, $E_2 = 0.9\times10^6$ kN/m^2, $N_{0x} = N_{0y} = 10$ kN/m, v_0 = 15 m/s. The boundary size of

Table 7 Comparison of maximum displacements for different membrane sizes

Number	1	2	3	4	5	6	7	8
Boundary size (mm × mm)	1000×500	900×450	800×400	700×350	600×300	400×200	300×150	200×100
Analytical results (mm)	1.4578	1.6199	1.8217	1.9273	1.942	1.9401	1.9375	1.93
Numerical results (mm)	2.1492	2.0438	2.0867	2.0401	2.0299	2.0609	2.0726	2.01
Relative difference	32.17%	20.74%	12.7%	5.53%	4.33%	5.85%	6.52%	3.98%

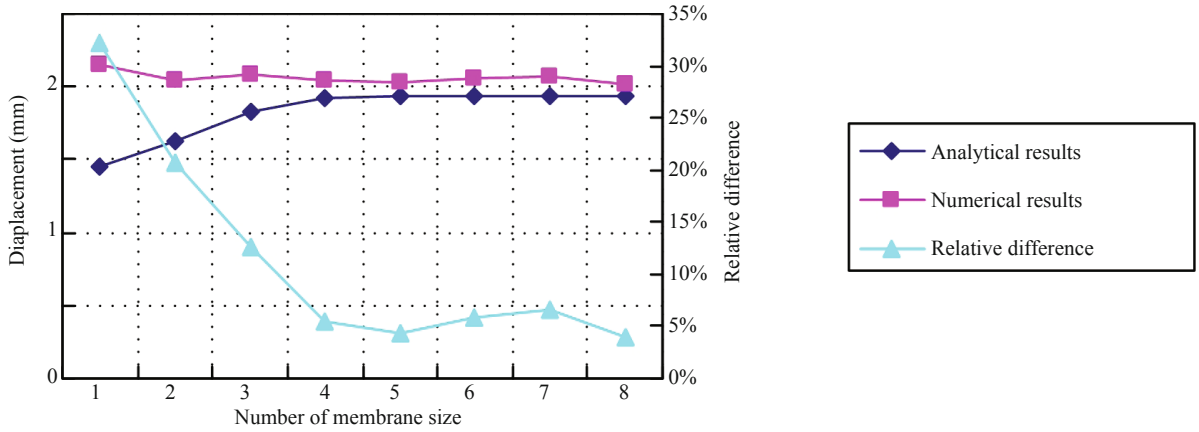

Fig. 16 Relative difference between analytical and numerical maximum displacements (membrane size number refers to membrane dimensions in Table 7)

the membrane is varied as shown in Table 7.

From Table 7 and Fig. 16, it can be seen that the differences between the analytical and numerical results gradually decrease with the decrease of membrane size. When the membrane size is smaller than 700mm×350mm (membrane size #4 or higher in Table 7), the relative differences stabilize at about 5%, which is acceptable engineering error.

6.2 Membrane pretension

Maximum displacements of the membrane under the impact pellet for selected membrane pretensions are calculated. The pretensions investigated are 5, 6, .. 10 kN, corresponding to pretension membrane number #1 through 6 in Table 8. The other parameters are $E_1 = 1.4\times10^6$ kN/m^2, $E_2 = 0.9\times10^6$ kN/m^2, a = 0.4 m, $b = 0.2$ m, $\rho = 1.7$kg/m^2, $h = 1$ mm, $M = 10^{-3}$kg, $v_0 = 15$ m/s. Analytical and numerical results on the maximum membrane displacement are collected in Table 8 and Fig. 17.

From Table 8 and Fig. 17, it can be seen that the differences between the analytical and numerical results gradually increase with increasing pretensions. The reason is that the actual vibration deformation is closer to the theoretical mode function when pretension is small, other parameters being held fixed; with decreasing pretension. the vibration mode approaches a sinusoidal function, the theoretical mode function.

6.3 Pellet velocity

Maximum displacements of the membrane under the impact of the pellet with different impact velocities were calculated. The velocities investigated are v_0 = 15, 17, 20, 25 and 27 m/s. The other parameters are $E_1 = 1.4\times10^6$ kN/m^2,

Table 8 Comparison of maximum displacements for different pretensions

Number	1	2	3	4	5	6
Pretension levels	N = 5 kN	N = 6 kN	N = 7 kN	N = 8 kN	N = 9 kN	N = 10 kN
Analytical results (mm)	2.7440	2.5049	2.3189	2.1692	2.0449	1.9401
Numerical results (mm)	2.7818	2.5695	2.4379	2.2704	2.1551	2.0609
Relative difference	1.36%	2.52%	4.88%	4.46%	5.11%	5.86%

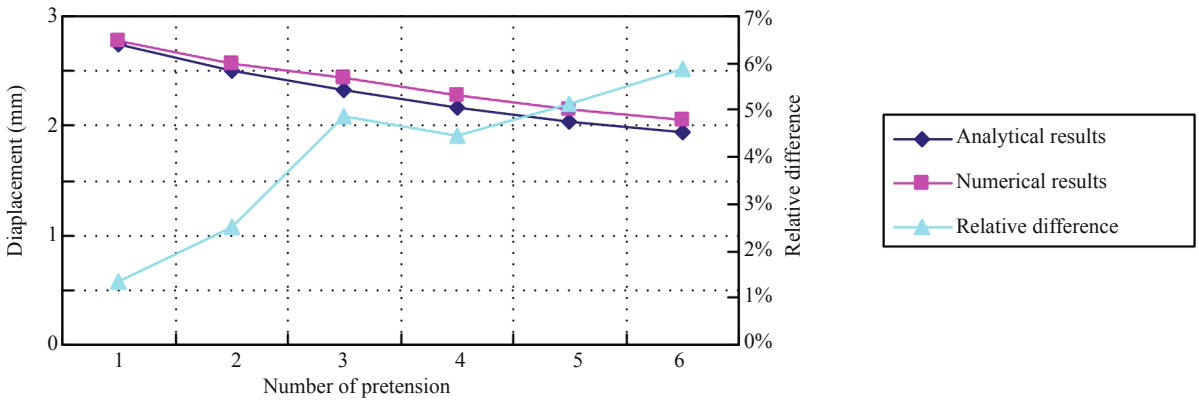

Fig. 17 Comparison of analytical and numerical maximum displacements of the membrane under different pretensions (pretension number refers to selected pretensions listed Table 8)

Table 9 Analytical and numerical maximum displacements with different pellet velocities

Number	1	2	3	4	5
Pellet velocities	v_0 = 15 m/s	v_0 = 17 m/s	v_0 = 20 m/s	v_0 = 25 m/s	v_0 = 27 m/s
Analytical results(mm)	1.455	1.6512	1.94	2.425	2.6213
Numerical results(mm)	1.6453	1.7957	2.0609	2.5527	2.7435
Relative difference	11.56%	8.04%	5.86%	5.00%	4.45%

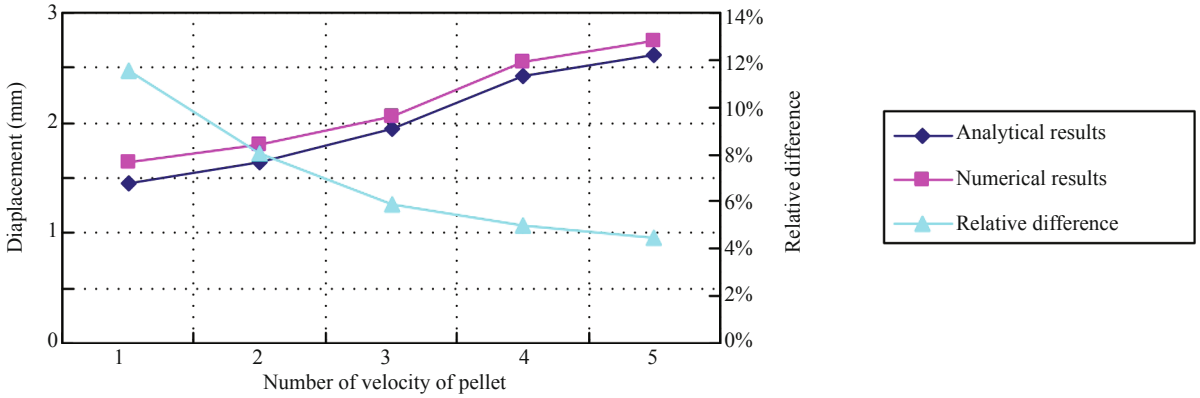

Fig. 18 Comparison of theoretical and numerical maximum displacements of impact point for different pellet velocities (pellet velocity number refers to values in Table 9)

$E_2 = 0.9\times10^6$ kN/m^2, a = 0.4 m, b = 0.2 m, ρ = 1.7 kg/m^2, h = 1 mm, M = 10^{-3} kg, $N_{0x} = N_{0y} = 10$ kN/m. The analytical and numerical results are compared in Table 9 and Fig. 18.

From Table 9 and Fig. 18, it can be seen that maximum displacement of the membrane increases with increasing pellet velocity, as expected. The difference between the analytical and numerical results gradually decreases with increasing pellet velocity. The reason is the same as the effect of membrane pretension described previously: the actual vibration deformation approaches the theoretical sinusoidal mode function as the pellet velocity increases, with the other parameters held fixed.

6.4 Areal density of the membrane

Maximum displacements of the membrane for areal densities varying between 1.0 kg/m^2 and 2.0 kg/m^2 were calculated. The other parameters are v_0 = 15 m/s, $E_1 = 1.4\times10^6$ kN/m^2, $N_{0x} = N_{0y} = 10$ kN/m, $E_2 = 0.9\times10^6$ kN/m^2, a = 0.4 m, b = 0.2 m, h = 1 mm, M = 10^{-3} kg. The analytical and numerical results are

Table 10 Analytical and numerical maximum displacements with different areal densities

Number	1	2	3	4	5
Areal densities	ρ = 1.0 kg/m^2	ρ = 1.2 kg/m^2	ρ = 1.5 kg/m^2	ρ = 1.7 kg/m^2	ρ = 2.0 kg/m^2
Analytical results (mm)	2.5244	2.3077	2.0668	1.9401	1.7871
Numerical results (mm)	2.5785	2.3812	2.2081	2.0609	1.8629
Relative difference	2.1%	3.09%	6.4%	5.86%	4.07%

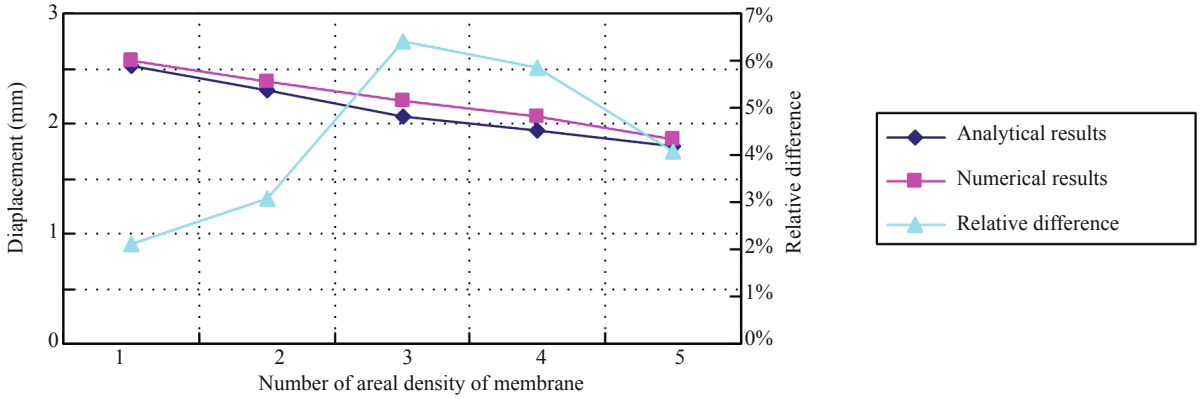

Fig. 19 The comparison of the analytical and numerical maximum displacement of the membrane with different area densities

shown in Table 10 and Fig. 19.

From Table 10 and Fig. 19, it can be seen that maximum displacements of the membrane decrease with increasing areal density. The reason is that initial velocity of the membrane will decrease with increasing areal density, according to the law of conservation of momentum. Differences between analytical and numerical results gradually increase with increase in areal density. The reason is again the same as aforementioned: the difference between the theoretical sinusoidal mode function and the actual membrane deformation will increase with decreasing areal density.

6.5 Pellet mass

Pellet masses considered are 0.8 g, 1.0 g, 1.2 g, 1.4 g and 1.6 g. The other parameters are v_0 = 15 m/s, $E_1 = 1.4\times10^6$ kN/m^2, $N_{0x} = N_{0y} = 10$ kN/m, $E_2 = 0.9\times10^6$ kN/m^2, a = 0.4 m, b = 0.2 m, ρ = 1.7 kg/m^2, h = 1 mm. Analytical and numerical results for the maximum displacement of the membrane are shown in Table 11 and Fig. 20.

From Table 11 and Fig. 20, it can be seen that the maximum displacements of the membrane increase with the increase of the mass of the pellet. The reason is that the impact energy of the pellet increases with the increasing pellet mass when pellet velocity is constant. Meanwhile, difference between the analytical and numerical results gradually decreases with increasing pellet mass because the difference between the theoretical sinusoidal mode function and the actual membrane deformation becomes smaller with increasing pellet mass.

6.6 The influence of the Young's modulus ratio

Assume that $E_1 = 1.4\times10^6$ kN/m^2, we varied E_2 from 0.7×10^6 kN/m^2 to 1.1×10^6 kN/m^2. The other parameters are v_0 = 15 m/s, M = 10^{-3} kg, $N_{0x} = N_{0y} = 10$ kN/m, a = 0.4 m, b = 0.2 m, ρ = 1.7 kg/m^2, h = 1 mm. Analytical and numerical results for maximum membrane displacement for various E_1/E_2 ratios are shown in Table 12 and Fig. 21.

From Table 12 and Fig. 21, it can be seen that maximum displacements of the membrane increase with the increase of Young's modulus ratios. This is because the increase of Young's modulus ratios with E_1 held constant means the decease of E_2 and the deformation of forced body will increase when Young's modulus

Table 11 Analytical and numerical maximum displacements for different pellet masses

Number	1	2	3	4	5
Pellet masses	M = 0.8 g	M = 1.0 g	M = 1.2 g	M = 1.4 g	M = 1.6 g
Analytical results (mm)	1.554	1.9401	2.3283	2.7132	3.1002
Numerical results (mm)	1.7021	2.0609	2.4576	2.7901	3.1716
Relative difference	8.70%	5.86%	5.26%	2.76%	2.25%

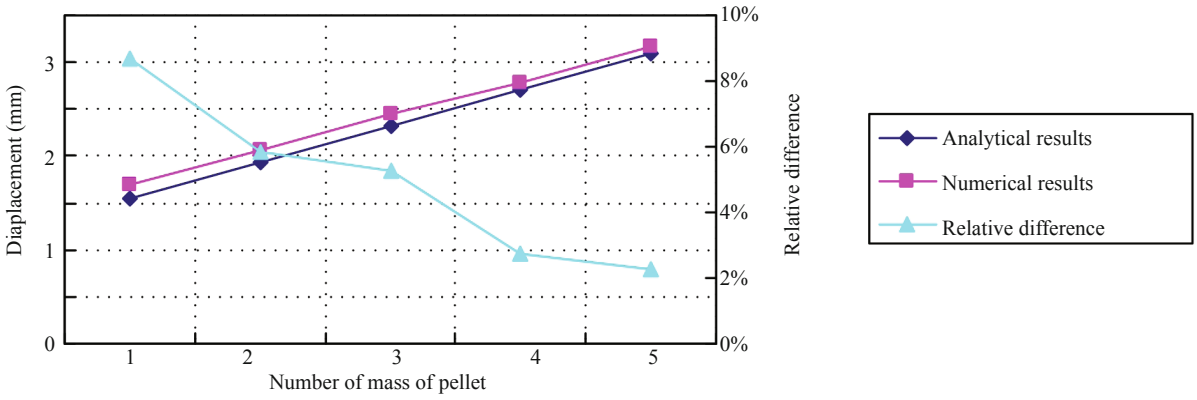

Fig. 20 Comparison of analytical and numerical maximum displacements of the membrane under different pellet masses (mass number refers to Table 11)

Table 12 Analytical and numerical maximum displacements for different pellet masses

Number	1	2	3	4	5
Young's modulus $\times 10^6$ kN/m^2	E_2 = 0.7	E_2 = 0.8	E_2 = 0.9	E_2 = 1.0	E_2 = 1.1
Analytical results (mm)	2.5971	2.2661	1.9401	1.6204	1.3142
Numerical results (mm)	2.7747	2.4138	2.0609	1.7005	1.3640
Relative difference	6.40%	6.12%	5.86%	4.71%	3.65%

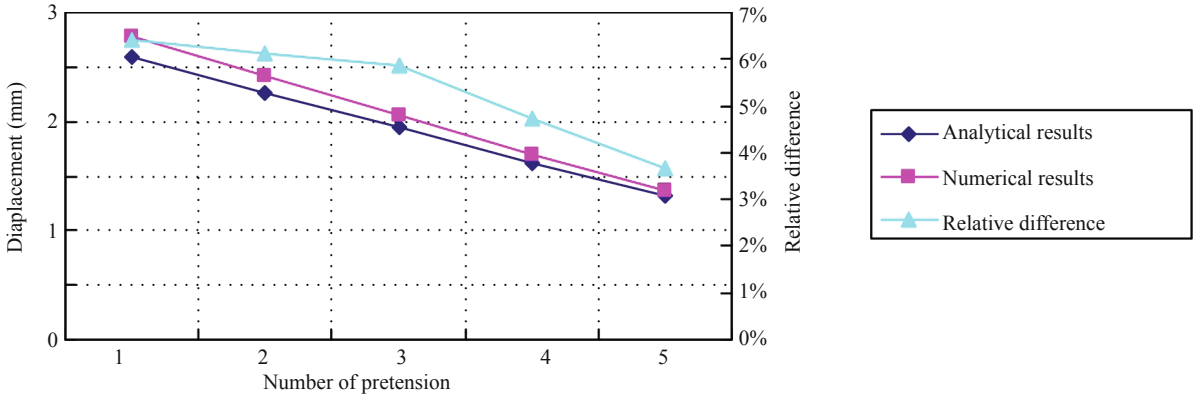

Fig. 21 Comparison of analytical and numerical maximum displacements of the membrane for different Young's modulus ratios (Young's modulus number refers to Table 12)

becomes smaller. Meanwhile, the difference between the analytical and numerical results gradually decreases with the decrease of Young's modulus ratio. The difference between the theoretical and numerical models will decrease when the Young's modulus ratio (E_1/E_2) approaches zero.

7 Conclusions

The nonlinear vibration response of an orthotropic membrane under concentrated impact load was studied with analytical and numerical methods in this paper. The governing equations were established by Von Kármán's large deflection theory and the D'Alembert principle. The governing equations were solved by the Bubnov-Galerkin method combined with the Lindstedt-Poincaré perturbation method, and analytical solutions obtained.

The numerical study was carried out by using the finite-element analysis software ANSYS/LS-DYNA. The numerical results are found to be very close to the analytical results. Only the theoretical values of the maximum displacement of the impact point are slightly less than those from the numerical study. This proves the correctness of the analytical solution.

The influence of various model parameters (including boundary size, pretension and surface density of the membrane and the velocity and quality of the pellet) on the vibration of the membrane is analyzed, and significant conclusions are obtained, as follows:

(1) Differences between the analytical and numerical results of the maxim displacement gradually decrease with decreasing membrane size. When membrane size is smaller than 700 mm × 350 mm, the relative differences stabilize at about 5%, which is in accordance with the requirement of the engineering error.

(2) Differences between the analytical and numerical results of the maxim displacement increase gradually with increasing pretension.

(3) The maximum displacements of the membrane increase with increasing pellet velocity or mass, and decrease with increasing membrane areal density.

The results presented in this paper may contribute some insight towards vibration control and dynamic design of orthotropic membrane components and structures.

Acknowledgment

This work was supported by the National Natural Science Foundation of China (Project Number: 51178485) and the personnel development project for young and middle-aged key teachers of Chengdu University of Technology (Project Number: KYGG201303).

References

Buchholdt HA (1998), *An Introduction to Cable Roof Structures*, 2nd, Thomas Telford Ltd.

Chen Liqun and Liu Yanzhu (1997), "Survey of the Historical Developments of Vibration Mechanics," *Journal of Shanghai Jiaotong University*, **31**(7): 132–136. (in Chinese)

Chen Zhaoqing, Wu Yue and Sun Xiaoying (2015), "Research on the Added Mass of Open-type One-way Tensioned Membrane Structure in Uniform Flow," *Journal of Wind Engineering and Industrial Aerodynamics*, **137**: 69–77.

Gajbhiye Sachin C, Upadhyay Sanjay H and Harsha Suraj P (2015), "Nonlinear Vibration Analysis of Piezo-actuated Flat Thin Membrane," *Journal of Vibration and Control*, **21**(6): 1162–1170.

Glück M, Breuer M, Durst F, Halfmann A and Rank E (2003), "Computation of Wind-induced Vibrations of Flexible Shells and Membranous Structures," *Journal of Fluids and Structures*, **17**(5): 739–765.

Khan Farid, Sassani Farrokh and Stoeber Boris (2014), "Nonlinear Behaviour of Membrane Type Electromagnetic Energy Harvester under Harmonic and Random Vibrations," *Microsystem Technologies*, **20**(7): 1323–1335.

Leigh Phoenix S and Porwal Pankaj K (2003), "A new Membrane Model for the Ballistic Impact Response and V50 Performance of Multi-ply Fibrous Systems," *International Journal of Solids and Structures*, **40**(24): 6723–6765.

Lin Wenjing, Chen Shuhui and Zhang Qiming (2008), "The Analytical Solution of Free Vibration of Annular Membrane," *Zhongshan Daxue Xuebao/Acta Scientiarum Natralium Universitatis Sunyatseni*, **47**(2): 103–108. (in Chinese)

Liu Changjiang, Yang Xiaoyan, Zhao Hua and Zheng Zhoulian (2014), "Homotopy Perturbation Solution for Strong Geometrical Nonlinear Vibration of Flat Prestressed Orthotropic Membrane Structure," *Shell Structures: Theory and Applications - Proceedings of the 10th SSTA 2013 Conference*, **3**: 313–316.

Liu Changjiang, Zheng Zhoulian, He Xiaoting, Sun Junyi, Song Weiju, Xu Yunping and Long Jun (2010), "L-P Perturbation Solution of Nonlinear Free Vibration of Prestressed Orthotropic Membrane in Large Amplitude," *Mathematical Problems in Engineering*, Article ID 561364, 17 pages.

Liu Changjiang, Zheng Zhoulian, Long Jun, Guo JianJun and Wu Kui (2013), "Dynamic Analysis for Nonlinear Vibration of Prestressed Orthotropic Membrane Structure with Viscous Damping," *International Journal of Structural Stability and Dynamics*, **13**(2), Article ID 1350018, 32 pages.

Liu Changjiang, Zheng Zhoulian, Yang Xiaoyan and Zhao Hua (2014), "Nonlinear Damped Vibration of Pre-stressed Orthotropic Membrane Structure under Impact Loading," *International Journal of Structural Stability and Dynamics*, **14**(1), Article ID 1350055, 24 pages.

Matsumoto T (1990), "Self-excited Oscillation of a Pretensioned Cable Roof with Single Curvature in Smooth Flow," *Journal of Wind Engineering and Industrial Aerodynamics*, **34**(3): 303–304.

Qian Guozhen (1982), "Solution for Free Vibration Problem of the Membrane with Unequal Tension in Two Directions," *Applied Mathematics and Mechanics*, **3**(6): 817–824.

Qin Jingwei, Yang Qingshan and Tan Feng (2008), "Dynamic Characteristics of Tensioned Cable-membrane Structures," *Spatial Structures*, **14**(2): 42–47. (in Chinese)

Shen Shizhao and Wu Yue (2006), "Research Progress on Fluid-solid Interaction Effect of Wind-induced Vibration Response of Membrane Structure," *Journal of Architecture and Civil Engineering*, **23**(1): 1–9.

Suhir E, Vujosevic M and Reinikainen T (2009), "Nonlinear Dynamic Response of a 'Flexible-and-heavy' Printed Circuit Board (PCB) to an Impact Load Applied to Its Support Contour," *Journal of Physics D: Applied Physics*, **42**(4): 45506–45515.

Sunny Mohammed R, Kapania Rakesh K and Sultan Cornel (2012), "Solution of Nonlinear Vibration Problem of a Prestressed Membrane by Adomian Decomposition," *AIAA Journal*, **50**(8): 1796–1800.

Wetherhold Robert and Padliya Punit S (2014), "Design Aspects of Nonlinear Vibration Analysis of Rectangular Orthotropic Membranes," *Journal of Vibration and Acoustics*, **136**(3), Article ID 034506, 4 pages.

Wu Yue and Shen Shizhao (2003), "Computational Simulation on Wind-induced Vibration of Membrane Structures," *Spatial Structures*, **9**(2): 38–43. (in Chinese)

Yasui H, Marukawa H, Katagiri J, Katsumura A, Tamura Y and Watanabe K (1999), "Study of Wind-induced Response of Long-span Structure," *Journal of Wind Engineering and Industrial Aerodynamics*, **83**(1–4): 277–288.

York II Allen R, Sulsky Deborah and Schreyer Howard L (1999), "Material Point Method for Simulation of Thin Membranes," *International Journal for Numerical Methods in Engineering*, **44**(10): 1429–1456.

Yuan Si and Zhang Yiguo (1993a), "Analysis of Nonlinear Model Problems by the Finite Element Method of Lines-I. Large Deflection of Membranes," *Engineering Mechanics*, **10**(1): 1–9. (in Chinese)

Yuan Si and Zhang Yiguo (1993b), "Analysis of Nonlinear Model Problems by the Finite Element Method of Lines-III, Free Vibration of Membranes," *Engineering Mechanics*, **10**(3): 1–8. (in Chinese)

Zheng Zhoulian, Liu Changjiang, He Xiaoting and Chen Shanlin (2009), "Free Vibration Analysis of Rectangular Orthotropic Membranes in Large Deflection," *Mathematical Problems in Engineering*, Article ID 634362, 9 pages.

Zheng Zhoulian, Song Weiju, Liu Changjiang, He Xiaoting, Sun Junyi and Xu Yunping (2012), "Study on Dynamic Response of Rectangular Orthotropic Membranes under Impact Loading," *Journal of Adhesion Science and Technology*, **26** (10–11): 1467–1479.

Zhou Xuanyi, Han Zhihui and Gu Ming (2013), "Research on Wind-induced Responses of a Large-scale Membrane Structure," *Earthquake Engineering and Engineering Vibration*, **12**(2): 297–305.